

Chiral twodimensional p -wave superfluid from s -wave pairing in the BEC regime

K. Thompson,^{1,2} J. Brand,^{3,2} and U. Zülicke^{1,2,4,*}

¹*School of Chemical and Physical Sciences, Victoria University of Wellington, PO Box 600, Wellington 6140, New Zealand*

²*Dodd-Walls Centre for Photonic and Quantum Technologies, PO Box 56, Dunedin 9056, New Zealand*

³*Centre for Theoretical Chemistry and Physics, and New Zealand Institute for Advanced Study, Massey University, Private Bag 102904 NSMC, Auckland 0745, New Zealand*

⁴*Department of Physics, University of Basel, Klingelbergstrasse 82, CH-4056 Basel, Switzerland*

(Dated: December 20, 2019)

Twodimensional spin-orbit-coupled Fermi gases subject to s -wave pairing can be driven into a topological phase by increasing the Zeeman spin splitting beyond a critical value. In the topological phase, the system exhibits the hallmarks of chiral p -wave superfluidity, including exotic Majorana excitations. Previous theoretical studies of this realization of a twodimensional topological Fermi superfluid have focused on the BCS regime where the s -wave Cooper pairs are only weakly bound and, hence, the induced chiral p -wave order parameter has a small magnitude. Motivated by the goal to identify potential new ways for the experimental realization of robust topological superfluids in ultra-cold atom gases, we study the BCS-to-BEC crossover driven by increasing the Cooper-pair binding energy for this system. In particular, we obtain phase diagrams in the parameter space of two-particle bound-state energy and Zeeman spin-splitting energy. Ordinary characteristics of the BCS-to-BEC crossover, in particular the shrinking and eventual disappearance of the Fermi surface, are observed in the nontopological phase. In contrast, the topological phase retains all features of chiral p -wave superfluidity, including a well-defined underlying Fermi surface, even for large s -wave pair-binding energies. Compared to the BCS limit, the topological superfluid in the BEC regime turns out to be better realizable even for only moderate magnitude of spin-orbit coupling because the chiral p -wave order parameter is generally larger and remnants of s -wave pairing are suppressed. We identify optimal parameter ranges that can aid further experimental investigations and elucidate the underlying physical reason for the persistence of the chiral p -wave superfluid.

I. INTRODUCTION AND OVERVIEW OF MAIN RESULTS

One of the earliest proposed pathways towards realization of a twodimensional (2D) topological superfluid (TSF) [1] is based on s -wave pairing of spin- $\frac{1}{2}$ fermions subject to spin-orbit coupling and Zeeman spin splitting [2–6]. In the absence of spin-orbit coupling, a population imbalance in the spin components (equivalent to nonzero Zeeman splitting) tends to destroy s -wave superfluidity due to the mismatch of the spin- \uparrow and spin- \downarrow Fermi surfaces for weak-coupling superfluids [7, 8]. With strong s -wave attraction, phase separation between superfluid and normal phases ensues in this case [9]. Adding 2D spin-orbit coupling (e.g., of Rashba form [10–12]) permits a pairing instability even for unmatched Fermi surfaces and re-establishes a homogeneous superfluid ground state with gapped fermionic quasiparticle excitations. The pairing field for each spin component separately [13] now obtains the characteristics of a chiral 2D p -wave superfluid [14]. Increasing the Zeeman coupling energy h beyond the critical value

$$h_c = \sqrt{\mu^2 + |\Delta|^2} \quad (1)$$

quenches one of the Fermi surfaces, and the system enters a TSF phase. In Eq. (1), Δ and μ denote the selfconsis-

tent s -wave pair potential and chemical potential, respectively. Bearing all the characteristics of a 2D spinless p -wave superfluid, a nontrivial topological invariant can be defined [1], and Majorana quasiparticle excitations are present at boundaries [2, 15] and in vortex cores [16–20] by virtue of an index theorem [21]. Majorana zero modes are considered promising candidates for enabling fault-tolerant quantum-information processing [22].

Intense efforts towards experimental implementation of 2D TSFs using the above-described route have so far been thwarted by the deleterious effect of Zeeman-splitting-inducing magnetic fields on superconductivity in typical materials [23], as well as basic physical constraints on the magnitude of spin-orbit coupling reachable in solids [11] and ultra-cold atom gases [24, 25]. Our present study shows that a possible way around the latter limitation would be to access the strong-coupling regime of the s -wave pairing, which is commonly referred to as the BEC regime [26–30].

The main insights reached in our work are underpinned by zero-temperature phase diagrams in the parameter space of two-particle s -wave bound-state energy E_b [31] and Zeeman energy h as illustrated in Fig. 1. These show a second-order transition line (red) between the nontopological and topological superfluids at small E_b being replaced by a first-order phase transition at larger E_b . In the phase diagram at constant particle density n , enforced by measuring energies in terms of the Fermi energy $E_F = \pi\hbar^2 n/m$, the first-order phase transition manifests itself as a region without a uniform-density ground state (grey) where phase separation into spatially sepa-

* uli.zuelicke@vuw.ac.nz

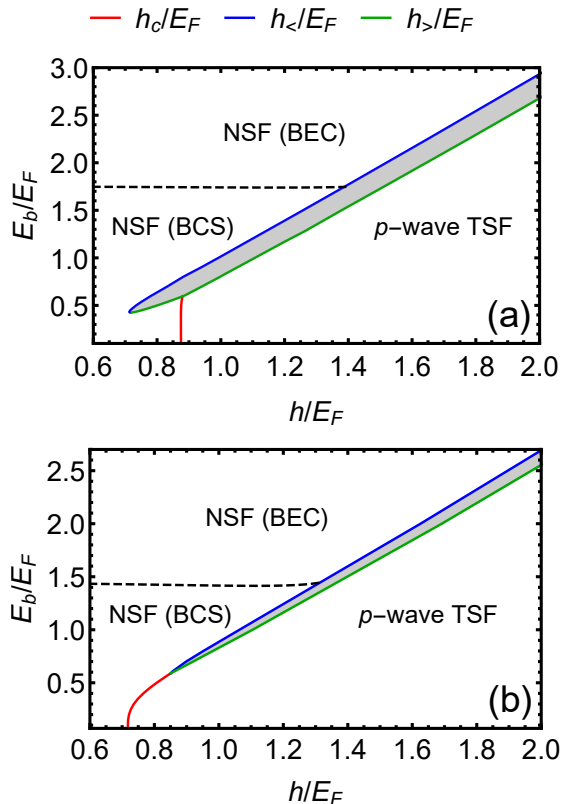


FIG. 1. Zero-temperature mean-field phase diagrams, in the parameter space of two-particle s -wave bound-state energy E_b and Zeeman energy h , for a spin-orbit-coupled 2D Fermi gas with fixed density $n = mE_F/(\pi\hbar^2) \equiv k_F^2/(2\pi)$. Panel (a) [(b)] depicts the case where the dimensionless parameter $\lambda k_F/E_F$ measuring the spin-orbit-coupling strength equals 0.50 [0.75], which illustrates a small-(large)-spin-orbit-coupling situation. The shaded region $h_< < h < h_>$, with $h_<$ ($h_>$) indicated by the blue (green) line, is in the phase-separated first-order-transition regime that emerges for $E_b > E_b^{(c)}$ and $h > h^{(c)}$. The critical Zeeman energy h_c , defined via Eq. (1) and indicated by the red curve, delineates the second-order transition between an ordinary nontopological superfluid (NSF) and a topological superfluid (TSF). From the point when the $h_c(E_b)$ -curve reaches the region where phase separation occurs, the topological transition is switched from second to first order. The BCS-to-BEC-crossover boundary (dashed line) has been determined via the condition $\mu(E_b, h) = 0$.

rated domains ensues. Critical Zeeman-energy values $h_<$ (blue) and $h_>$ (green) delimit the phase-separation region at fixed E_b , defining two curves in the phase diagram. The properties of the phase-separation region itself have been the subject of previous work [32, 33], and we also provide a few more details later on. However, the main focus of our present study is the careful determination of the location of the boundaries $h_<$ and $h_>$ and the exploration of the adjacent homogeneous phases, especially in the regime where $E_b/E_F \gtrsim 1$.

Comparison of our results with those obtained previously for spin-imbalanced 2D Fermi superfluids [34] helps

to elucidate the physical consequences of finite spin-orbit coupling. The magnitude of the latter is most conveniently measured in terms of the dimensionless parameter $\lambda k_F/E_F$ that also involves the density-dependent Fermi wave number $k_F \equiv \sqrt{2\pi n}$. One important effect of finite λ is to shift the low- E_b boundary of the phase-separation region from zero to finite values of E_b [9], and a second effect is to establish the TSF phase [33] for sufficiently high Zeeman energy $h > \max\{h_c, h_>\}$ in place of the fully polarized normal phase found for $\lambda = 0$ [9].

Our present study shows that the character of the TSF phase emerging in the BEC regime of the underpinning s -wave pairing ($E_b/E_F \gtrsim 1$) is fundamentally similar to the TSF occurring in the BCS limit ($E_b/E_F \ll 1$). In particular, for the entire TSF region in the phase diagram, the system exhibits canonical signatures of an underlying Fermi surface. As discussed by Sensarma *et al.* [35], an underlying Fermi surface can be robustly defined even in strong-coupling fermionic superfluids by a number of alternative definitions, such as a zero crossing of the single-particle Greens function $G(\mathbf{k}, 0)$, a drop in the single-particle momentum distribution $n(\mathbf{k})$, or, if available, by a minimum of the quasiparticle dispersion relation. Our results for the TSF are in stark contrast to the nontopological superfluid (NSF) phase where the Fermi surface shrinks and eventually disappears as E_b/E_F increases and the BEC regime is entered. This is expected from the known phenomenology of the BCS-to-BEC crossover for s -wave pairing [36–38] and illustrated by recent Quantum-Monte-Carlo results [39, 40].

The defining element of the 2D TSF is an emergent chiral p -wave order parameter Δ_{pw} whose magnitude provides the energy scale of the quasiparticle-excitation gap. Its value is proportional to the spin-orbit-coupling strength λ and the modulus $|\Delta|$ of the s -wave pair potential, but inversely related to the spin-splitting (Zeeman) energy scale h [3, 5, 6, 13, 41]. Given that increasing λ has adverse side effects such as heating of the atom gas [24] in currently available experimental schemes, maximizing Δ_{pw} needs to be pursued by other means. As $|\Delta|/E_F$ is a monotonously increasing function of E_b/E_F but is suppressed with increasing h/E_F (see, e.g., Refs. [13, 42] and below), its practically largest magnitude occurs just after the transition to the homogeneous TSF phase at $h_{\max} = \max\{h_c, h_>\}$. Figure 2(a) illustrates the dependence of this value, $|\Delta|_{h=h_{\max}}$, on both E_b and λ . It reveals a maximum that gets broader and larger as the parameter $\lambda k_F/E_F$ increases. As the maximum value of $|\Delta|$ reaches values up to $\sim E_F$ typically, even for only moderately high values of the spin-orbit-coupling strength, the TSF realized in the BEC regime of s -wave pairing presents a much more favorable platform for useful study and application than would be available in the BCS regime at the same value of λ . This is established even more directly by measuring Δ_{pw} as the gap in the low-energy quasiparticle dispersion for the TSF. The values for Δ_{pw} found for the same parameter combinations that maximize $|\Delta|$ are shown in Fig. 2(b). For both

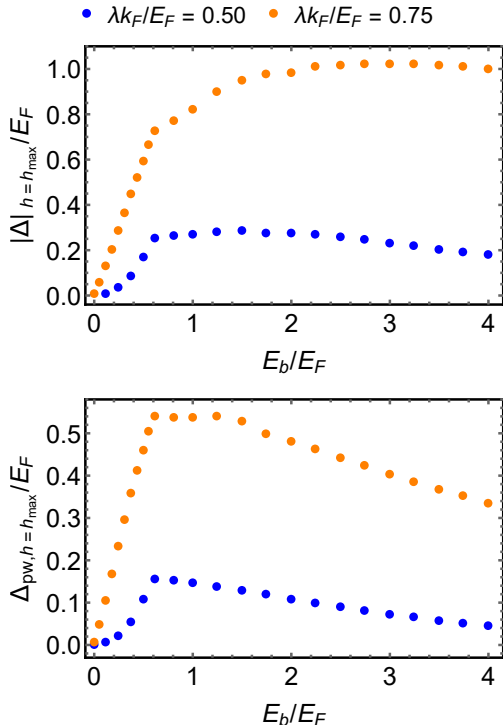


FIG. 2. The magnitude of the s -wave pair potential Δ in the homogeneous topological-superfluid phase of a spin-orbit-coupled 2D Fermi gas with fixed density $n = mE_F/(\pi\hbar^2) \equiv k_F^2/(2\pi)$ is maximized, for fixed two-particle bound-state energy E_b and spin-orbit-coupling strength λ , right after the transition at Zeeman energy $h_{\max} = \max\{h_c, h_\>\}$ (see Fig. 1). Panel (a) shows the dependence of this maximum value, $|\Delta|_{h=h_{\max}}$, on E_b for two fixed values of the dimensionless spin-orbit-coupling strength $\lambda k_F/E_F$. Panel (b) is a plot of the emergent chiral- p -wave gap Δ_{pw} , extracted from the low-energy quasiparticle dispersion, for the same parameters.

fixed values of $\lambda k_F/E_F$, a maximum of Δ_{pw} occurs for $E_b/E_F \sim 1$, followed by a broad range for which Δ_{pw} is slowly decreasing.

All quantitative results in this work were obtained within mean-field theory, even though its validity for a 2D gas, in particular outside of the weakly interacting regime, may not be taken for granted. We nevertheless expect the qualitative physics, and in particular the presence of a Fermi surface in the TSF phase, to be robust because the topological property puts strong constraints on the many-body system. We comment further on the physical reasons below. Mean-field approximations have previously been found to provide useful insight into zero-temperature phases, even when interactions are strong [9, 43–45]. Quantitatively more accurate predictions, in particular for finite temperature, require more sophisticated approaches [43, 44, 46–51]. The expected effects of beyond-mean-field corrections (quantum fluctuations) is to suppress pairing gaps compared to mean-field theory in the strongly interacting regime [49, 51]. This fact reinforces the optimal value $E_b/E_F \sim 1$ for re-

alizing a robust TSF, as for $E_b/E_F \gg 1$, the true value for the s -wave pairing gap, and therefore also Δ_{pw} , are likely to be much smaller than mean-field theory predicts.

The physical reasons for the remarkable BCS-like behavior of the TSF even when interactions are strong enough to place s -wave pairs into the BEC regime may be seen from a careful analysis of the relevant low-energy part of the quasiparticle spectrum. A projection of the mean-field equations to the majority-spin component [13] yields a useful approximate expression for the excitation gap and TSF order parameter

$$\Delta_{\text{pw}} \approx |\Delta| \frac{\lambda k_{\text{FS}}}{h_{k_{\text{FS}}}}, \quad (2)$$

where $h_k = (h + \sqrt{h^2 + \lambda^2 k^2})/2$, and $k_{\text{FS}} \leq \sqrt{2}k_F$ is the radius of the Fermi surface in the TSF phase (see end of Sec. III). The projective approximation is valid when Δ_{pw} is small compared to the Fermi energy E_F , but this condition will be fulfilled when spin-orbit coupling is not too strong, $\lambda k_F < E_F$, in the TSF regime where $h > |\Delta|$ due to Eq. (1). Note that this means that Δ_{pw} is bounded while the binding energy E_b may be much larger. Within the same projective approximation [13] and for $\lambda k_F < h$, one also obtains the estimate

$$k_{\text{FS}} \approx k_F \left[\frac{\mu + h - \frac{|\Delta|^2}{2h}}{E_F \left(1 - \frac{1}{2} \frac{\lambda^2 k_F^2}{E_F h}\right)} \right]^{\frac{1}{2}}, \quad (3)$$

which shows that the Fermi surface radius is finite, $k_{\text{FS}} > 0$, as long as the Zeeman energy h is sufficiently large. Thus the large magnitude of the Zeeman energy required to reach the uniform TSF phase ultimately ensures the persistence of BCS-like character of chiral p -wave pairing, even as the s -wave interaction is deep in the BEC regime. While the situation becomes slightly more complex for very large spin-orbit-coupling strengths $\lambda k_F/E_F > 1$, we still find signatures of a Fermi surface persisting throughout the TSF phase, and canonical BCS-like behavior being exhibited for $h \gtrsim h_{\max}$.

The remainder of this article is organized as follows. Section II introduces the theoretical approach used by us to describe the BCS-to-BEC crossover for the s -wave-paired 2D Fermi gas subject to both spin-orbit coupling and Zeeman spin splitting. Detailed results obtained within this formalism for the system with fixed uniform particle density are presented in the subsequent Sec. III, together with a discussion of physical implications and limitations inherent in the mean-field approach. Our conclusions are formulated in the final Sec. IV.

II. MICROSCOPIC MODEL OF THE 2D TSF

We utilize a standard Bogoliubov-de Gennes (BdG) mean-field formalism [52] to calculate the quasiparticle spectrum for our system of interest. All relevant thermodynamic quantities can be expressed in terms of the

obtained eigenenergies and eigenstates. Throughout this work, we consider the zero-temperature limit.

The BdG Hamiltonian of the 2D spin-orbit coupled Fermi gas with s -wave interactions and Zeeman spin splitting $2h$ acting in the four-dimensional Nambu space of spin-1/2 fermions is [53]

$$\mathcal{H} = \begin{pmatrix} \epsilon_{\mathbf{k}\uparrow} - \mu & \lambda_{\mathbf{k}} & 0 & -\Delta \\ \lambda_{\mathbf{k}}^* & \epsilon_{\mathbf{k}\downarrow} - \mu & \Delta & 0 \\ 0 & \Delta^* & -\epsilon_{\mathbf{k}\uparrow} + \mu & \lambda_{\mathbf{k}}^* \\ -\Delta^* & 0 & \lambda_{\mathbf{k}} & -\epsilon_{\mathbf{k}\downarrow} + \mu \end{pmatrix}, \quad (4)$$

where $\mathbf{k} = (k_x, k_y)$ denotes the 2D wave vector, $\epsilon_{\mathbf{k}\uparrow(\downarrow)} = \epsilon_{\mathbf{k}} \mp h$ with $\epsilon_{\mathbf{k}} = \hbar^2(k_x^2 + k_y^2)/2m$, and $\lambda_{\mathbf{k}} \equiv \lambda i(k_x - ik_y)$ is the spin-orbit coupling [54]. The BdG equation reads

$$\mathcal{H} \begin{pmatrix} u^\uparrow \\ u^\downarrow \\ v^\uparrow \\ v^\downarrow \end{pmatrix} = E \begin{pmatrix} u^\uparrow \\ u^\downarrow \\ v^\uparrow \\ v^\downarrow \end{pmatrix}. \quad (5)$$

Its spectrum consists of four eigenvalue branches [32, 55],

$$E_{\mathbf{k}\alpha, <(>)} = \alpha \sqrt{(\epsilon_{\mathbf{k}} - \mu)^2 + |\Delta|^2 + h^2 + |\lambda_{\mathbf{k}}|^2} \mp 2\sqrt{(\epsilon_{\mathbf{k}} - \mu)^2(h^2 + |\lambda_{\mathbf{k}}|^2) + |\Delta|^2 h^2}, \quad (6)$$

with associated eigenspinors $(u_{\mathbf{k}\alpha, \eta}^\uparrow, u_{\mathbf{k}\alpha, \eta}^\downarrow, v_{\mathbf{k}\alpha, \eta}^\uparrow, v_{\mathbf{k}\alpha, \eta}^\downarrow)^T$, where $\alpha \in \{+, -\}$ and $\eta \in \{<, >\}$ label the four different energy-dispersion branches.

The chemical potential μ and magnitude $|\Delta|$ of the pair potential need to be determined selfconsistently from solutions of the BdG equations in conjunction with the gap equation and the constraint that the uniform particle density is fixed at $n \equiv k_F^2/(2\pi)$. Corresponding conditions can be formulated mathematically in terms of the energy spectrum and BdG-Hamiltonian eigenspinor amplitudes. See, e.g., Refs. [13, 52]. However, educated by the insights gained from previous work on spin-imbalanced Fermi superfluids [56], we base selfconsistency considerations on the properties of the system's grand-canonical ground-state energy density [32, 44, 55–57], for which a standard calculation yields

$$\mathcal{E}_{\text{gs}}^{(\text{MF})}(|\Delta|, \mu) = \frac{1}{A} \sum_{\mathbf{k}} \left(\frac{|\Delta|^2}{2\epsilon_{\mathbf{k}} + E_b} + \epsilon_{\mathbf{k}} - \mu - \frac{1}{2} \sum_{\eta} E_{\mathbf{k}+, \eta} \right). \quad (7)$$

Here A denotes the system's volume (area), and $E_b > 0$ is the magnitude of the two-particle bound-state (i.e., binding) energy [31]. The gap and number-density equations can be expressed in terms of derivatives of the ground-state energy density;

$$\frac{\partial \mathcal{E}_{\text{gs}}^{(\text{MF})}}{\partial |\Delta|} = 0, \quad (8a)$$

$$\frac{\partial \mathcal{E}_{\text{gs}}^{(\text{MF})}}{\partial \mu} = -n. \quad (8b)$$

The lengthy explicit expressions are omitted here.

As emphasized previously during the study of spin-imbalanced Fermi superfluids [58], proper application of the condition (8a) for identifying physical ground states requires ensuring that $\mathcal{E}_{\text{gs}}^{(\text{MF})}(|\Delta|, \mu)$, taken as a function of $|\Delta|$ at fixed μ , has a global minimum at the selfconsistently determined value for $|\Delta|$. However, identifying

local minima as well as maxima of the ground-state energy at fixed μ can also be of interest [59–61], e.g., to discuss nonequilibrium-dynamic phenomena; hence, we will track these in the following also.

The relative magnitude of E_b with respect to the Fermi energy E_F drives the BCS-to-BEC crossover for s -wave pairing in our system of interest [28]. More specifically, we have

$$\frac{E_b}{E_F} \begin{cases} \ll 1 & \text{in the BCS limit,} \\ \gtrsim 1 & \text{in the BEC regime.} \end{cases} \quad (9)$$

In the following, we absorb any dependence on total particle density n by measuring all energies and wave vectors in units of E_F and k_F , respectively. Thus the set of externally tuneable parameters comprises E_b/E_F , h/E_F , and $\lambda k_F/E_F$. The system's state is characterized by $|\Delta|/E_F$ and μ/E_F .

The chiral p -wave nature of the superfluid is revealed by the following considerations. Inspection of Eq. (6) shows that $E_{\mathbf{0}+, <} = |h_c - h|$. In the BCS regime, for $0 < h < h_c$, two minima exist in $E_{\mathbf{k}+, <}$ at $|\mathbf{k}| > 0$, corresponding to effective p -wave pairing around the two spin-split Fermi surfaces for spin- \uparrow and spin- \downarrow degrees of freedom. As h is increased, the location of the spin- \downarrow minimum moves towards $|\mathbf{k}| = 0$, with its value shrinking and finally vanishing as it reaches $|\mathbf{k}| = 0$ at $h = h_c$. For $h > h_c$, the system has only one Fermi surface corresponding to a fully polarized electron system, and the remaining minimum of $E_{\mathbf{k}+, <}$ at $|\mathbf{k}| \sim \sqrt{2}k_F$ is associated with an effective pair potential [6, 13] $(\lambda_{\mathbf{k}}/|\lambda_{\mathbf{k}}|) \Delta_{\text{pw}} \equiv ie^{-i\varphi_{\mathbf{k}}} \Delta_{\text{pw}}$, where $\varphi_{\mathbf{k}} = \arctan(k_y/k_x)$ is the polar-angle coordinate for the 2D wave vector \mathbf{k} . Proportionality of the superconducting order parameter to the phase factor $e^{-i\varphi_{\mathbf{k}}}$ is the defining property of chiral p -wave pairing [14], and also the origin of its accompanying topological features [1, 14]. In contrast, the system has *two* Fermi surfaces where p -wave pairing with *opposite* chirality occurs when $h < h_c$, rendering it to be a nontopological superfluid. We now apply the formalism introduced above

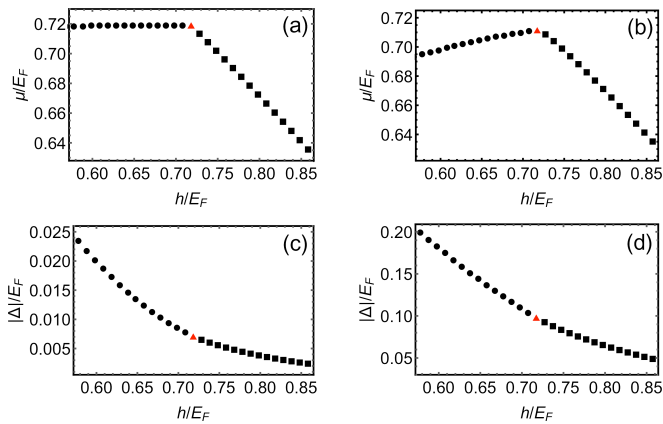


FIG. 3. Chemical potential μ and magnitude $|\Delta|$ of the s -wave pair potential for a spin-orbit-coupled 2D Fermi system with fixed density $n = mE_F/(\pi\hbar^2) \equiv k_F^2/(2\pi)$ in the BCS regime for s -wave pairing, plotted as a function of Zeeman splitting h . Results shown are obtained as solutions of the selfconsistency conditions [Eqs. (8a) and (8b)] for $\lambda k_F/E_F = 0.75$ (all panels) and $E_b/E_F = 0.010$ [panels (a) and (c)], 0.10 [panels (b) and (d)]. Data points indicated by circles (a triangle, squares) correspond to states where the system is nontopological (critical, topological), i.e., $h < (=, >) \sqrt{\mu^2 + |\Delta|^2}$.

to investigate the fate of chiral p -wave superfluidity in the BEC regime for the underlying s -wave pairing.

III. RESULTS AND DISCUSSION

To ground ourselves in well-known results [13, 42], we start by fixing a value for $\lambda k_F/E_F$ and consider the variation of the chemical potential μ and the pair-potential magnitude $|\Delta|$ as a function of the Zeeman energy h in the BCS limit for s -wave pairing, i.e., for small E_b/E_F . As illustrated in Fig. 3, both $\mu(h)$ and $|\Delta(h)|$ evolve continuously from the nontopological phase where $h < h_c$ [defined in Eq. (1)] via their critical values $\mu_c \equiv \mu(h_c)$ and $|\Delta(h_c)| \equiv \Delta_c$ that satisfy $\sqrt{\mu_c^2 + \Delta_c^2} = h_c$ into the topological phase where $h > h_c$. This reflects the fact that, for any value of h , $\mathcal{E}_{\text{gs}}^{(\text{MF})}$ has only a single minimum when plotted as a function of $|\Delta|$ for fixed μ , which occurs at a nonzero $|\Delta|$ and thus corresponds to a homogeneous superfluid ground state.

The search for solutions of the selfconsistency conditions (8a) and (8b) for larger $E_b/E_F \lesssim 1$ continues to yield unique values of $|\Delta|$ and μ . See the examples shown in Fig. 4. However, an intricate complexity associated with selfconsistent solutions starts to develop. As illustrated in Fig. 5, within an intermediate range of Zeeman energies, two additional extrema (specifically, a local minimum and a local maximum) start to appear in the $|\Delta|$ -dependence of the ground-state energy where μ has been fixed to its selfconsistent value. Below the value $E_b^{(c)}$ associated with the critical end-point of the phase-separation region shown in Fig. 1, the unique so-

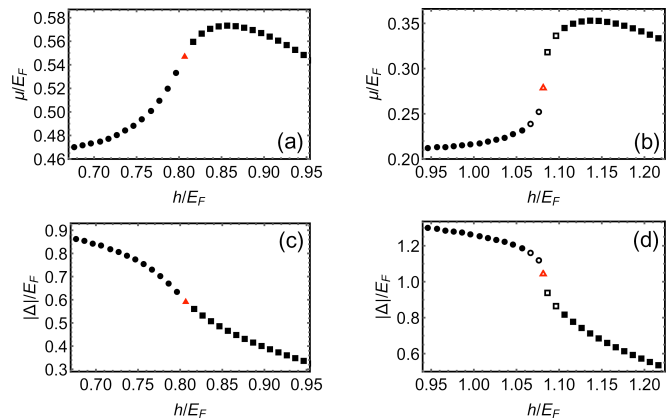


FIG. 4. Chemical potential μ and s -wave pair-potential magnitude $|\Delta|$ for a spin-orbit-coupled 2D Fermi system with fixed density approaching the BEC regime for s -wave pairing. Results shown are obtained as solutions of the selfconsistency conditions for $\lambda k_F/E_F = 0.75$ (all panels) and $E_b/E_F = 0.50$ [panels (a) and (c)], 1.0 [panels (b) and (d)]. Circles (a triangle, squares) correspond to states where the system is nontopological (critical, topological). Filled (empty) symbols indicate solutions of the selfconsistency conditions that globally minimize the ground-state energy and thus correspond to proper equilibrium states of the system (that represent only a local minimum or even a maximum of the ground-state energy).

lution of the selfconsistency conditions still continues to be the global minimum of $\mathcal{E}_{\text{gs}}^{(\text{MF})}$, taken at the selfconsistent μ , for any value of h . This is the case, e.g., for the system parameters used to calculate the results shown in Fig. 4(a,c). However, for $E_b \geq E_b^{(c)}$, which applies

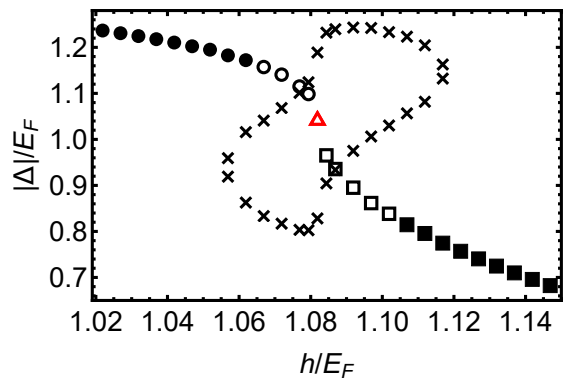


FIG. 5. Emergence of additional zeros of the gap equation in the BEC regime. Results shown are obtained for $\lambda k_F/E_F = 0.75$ and $E_b/E_F = 1.0$. Filled symbols indicate solutions of the selfconsistency conditions that globally minimize the ground-state energy and thus correspond to proper equilibrium states of the system. Empty symbols (crosses) are associated with (non)selfconsistent values corresponding to a local minimum or maximum of the ground-state energy. Circles (a triangle, squares) indicate selfconsistent solutions where the system is nontopological (critical, topological).

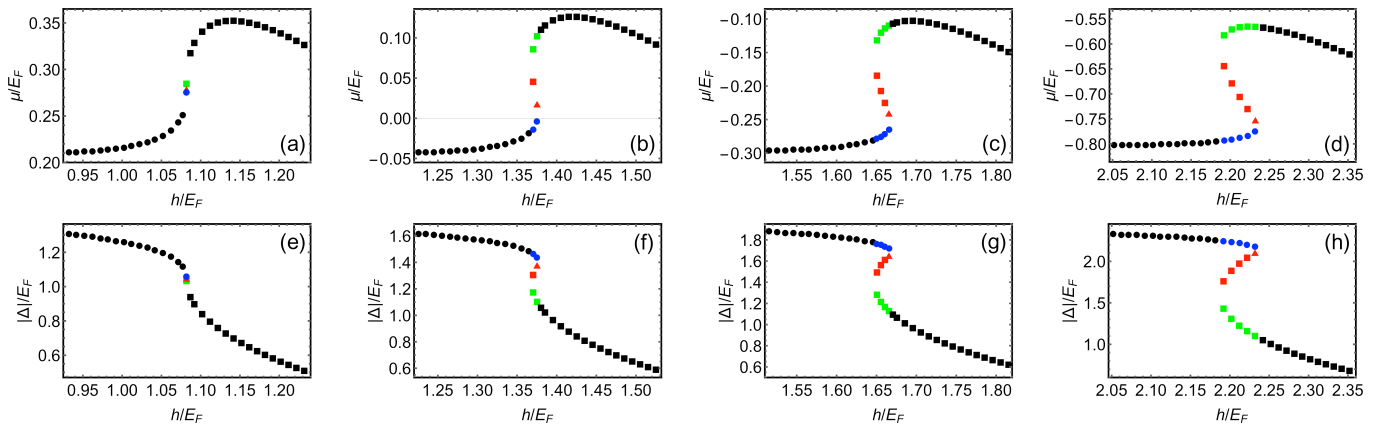


FIG. 6. Emergence of multiple pairs of selfconsistent solutions for the chemical potential μ and s -wave pair-potential magnitude $|\Delta|$, indicated by colors. Results shown here are obtained for $\lambda k_F/E_F = 0.75$ (all panels) and $E_b/E_F = 1.001$ [panels (a) and (e)], 1.5 [panels (b) and (f)], 2.0 [panels (c) and (g)], 3.0 [panels (d) and (h)]. Circles (a triangle, squares) correspond to states where the system is nontopological (critical, topological).

to Fig. 4(b,d), the selfconsistently determined value for $|\Delta|$ ceases to be associated with the global minimum of $\mathcal{E}_{\text{gs}}^{(\text{MF})}$ at fixed selfconsistent μ for Zeeman energies within a range $h_< < h < h_>$, corresponding instead to only a local minimum or even a maximum. This implies that no single-phase equilibrium ground state exists in the region $h_< < h < h_>$. Instead, phase separation into domains of different densities will occur if the system is driven into this region. Even further in the BEC regime when $E_b > E_b^{(\text{m})}$, multiple selfconsistent pairs of values for $|\Delta|$ and μ emerge as illustrated in Fig. 6. Around each of these, additional zeros of the gap equation exist, as seen in Fig. 7. Now the range $h_< < h < h_>$ is defined to be the region where none of the selfconsistent $|\Delta|$ values is associated with the global minimum of the ground-state energy $\mathcal{E}_{\text{gs}}^{(\text{MF})}$ when μ is fixed to its corresponding selfconsistent value.

The appearance of multiple extrema in the $|\Delta|$ dependence of $\mathcal{E}_{\text{gs}}^{(\text{MF})}$ at fixed μ , leading to the selfconsistent minimum ceasing to be the global minimum, indicates the presence of a first-order (noncontinuous) phase transition [9, 55]. A proper theoretical description of this situation requires the construction of various phase-coexistence scenarios [32, 33, 41], in analogy with treatments developed for the population-imbalanced Fermi gas without spin-orbit coupling [9, 44, 57, 62–66]. Here we defer the careful determination of the equilibrium ground state in the phase-separation region to future work [67]. Rather, we intend to discuss the properties of the adjacent uniform, single-phase regions for large E_b/E_F . To this end, we only need to map carefully the boundaries of the phase-separation region, i.e., the critical-Zeeman-energy curves $h_<$ and $h_>$. Results for representative values of the spin-orbit-coupling strength are given in Fig. 1. We find that the phase-separation region narrows as the spin-orbit-coupling parameter $\lambda k_F/E_F$ is increased, while simultaneously the

critical end point $(h^{(c)}, E_b^{(c)})$ where the $h_<$ and $h_>$ curves merge shifts to larger coordinate values in the phase diagram. The full dependence of $E_b^{(c)}$ (and also of $E_b^{(\text{m})}$) as a function of the dimensionless spin-orbit-coupling strength is plotted in Fig. 8(a), with the associated results for $h^{(c)}$ being provided in Fig. 8(b). Two different regimes, corresponding to small and large values of $\lambda k_F/E_F$, can be identified, where the former (latter) is characterized by the $h^{(c)}$ values diverging from (coinciding with) the critical field h_c for $E_b = E_b^{(c)}$.

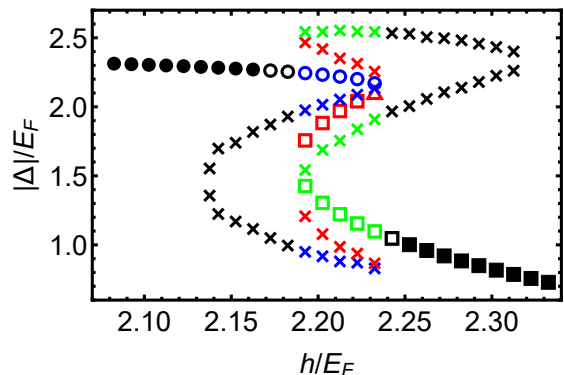


FIG. 7. Structure of multiple selfconsistent and associated nonselfconsistent solutions of the gap equation deep in the BEC regime. Results shown are obtained for $\lambda k_F/E_F = 0.75$ and $E_b/E_F = 3.0$. Filled symbols indicate solutions of the selfconsistency conditions that globally minimize the ground-state energy and thus correspond to proper equilibrium states of the system. Empty symbols (crosses) are associated with (non)selfconsistent values corresponding to a local minimum or maximum of the ground-state energy. Circles (a triangle, squares) indicate states where the system is nontopological (critical, topological). Multiple selfconsistent solutions at a given h are distinguished by color. The same color is used to indicate their associated additional zeros in the gap equation.

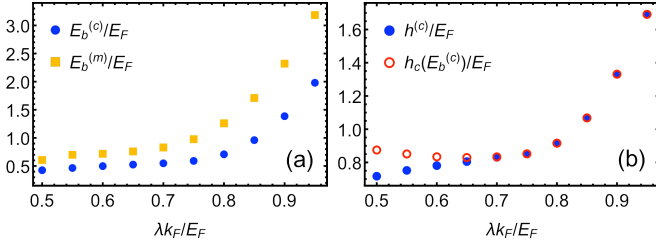


FIG. 8. Panel (a): Special values $E_b^{(c)}$ and $E_b^{(m)}$ for the two-particle bound-state energy E_b plotted as a function of the spin-orbit-coupling strength λ . Here $E_b^{(c)}$ is the value of E_b associated with the critical end point ($h^{(c)}$, $E_b^{(c)}$) of the phase-separation region in the E_b - h phase diagram where the critical-field curves $h_<$ and $h_>$ merge. The value $E_b^{(m)}$ is the lower limit of bound-state energies for which multiple pairs of selfconsistent solutions for μ and $|\Delta|$ exist. Panel (b): Dependence of $h^{(c)}$, the h coordinate of the critical end point of the phase-separation region in the E_b - h phase diagram, on the spin-orbit-coupling strength. For comparison, the critical field h_c [defined in Eq. (1)] at $E_b^{(c)}$ is also shown.

The curves for $h_<(E_b)$ and $h_>(E_b)$ in the phase diagram delimit the phase-separation region associated with a first-order transition between different superfluid states. In those parts of the phase diagram outside this region where only a single pair of selfconsistent values for μ and $|\Delta|$ exists, a curve $h_c(E_b)$ can be defined via Eq. (1) that separates the part of the phase diagram where the system is an ordinary nontopological superfluid (NSF, for $h < h_c$) from the part where the ground state corresponds to a topological superfluid (TSF, for $h > h_c$). In particular, for $E_b < E_b^{(c)}$, only this second-order topological transition occurs. However, beyond the point where the curve for $h_c(E_b)$ crosses that of $h_>(E_b)$, solutions of the selfconsistency conditions that are critical, i.e., satisfy $h = \sqrt{\mu^2 + |\Delta|^2}$, continue to exist but are no longer a global minimum of the ground-state energy at fixed μ . At the same time, the homogeneous-superfluid states existing for $h > h_>$ satisfy $h > \sqrt{\mu^2 + |\Delta|^2}$ and are thus in the topological phase. Hence, beyond the crossing point of $h_c(E_b)$ and $h_>(E_b)$, the topological transition is of first order. The phase boundary of the homogeneous 2D TSF is therefore delineated by $h_{\max}(E_b) = \max\{h_c(E_b), h_>(E_b)\}$. Due to the tendency of $|\Delta|$ to monotonically decrease with h in regions where a selfconsistent solution is associated with the system's equilibrium ground state (see Figs. 3, 5, and 7), h_{\max} is also the Zeeman energy for which $|\Delta|$ is maximized in the TSF phase at fixed E_b . We now focus on the properties of the single-phase ground states adjacent to the phase-separation region at large $E_b > E_b^{(c)}$.

The typical phenomenology of the BCS-to-BEC crossover for s -wave pairing entails a shift of the dispersion minimum to $k = 0$, Bogoliubov quasi-particles becoming mostly particle-like, and the momentum-space density distribution losing its typical Fermi-surface-like

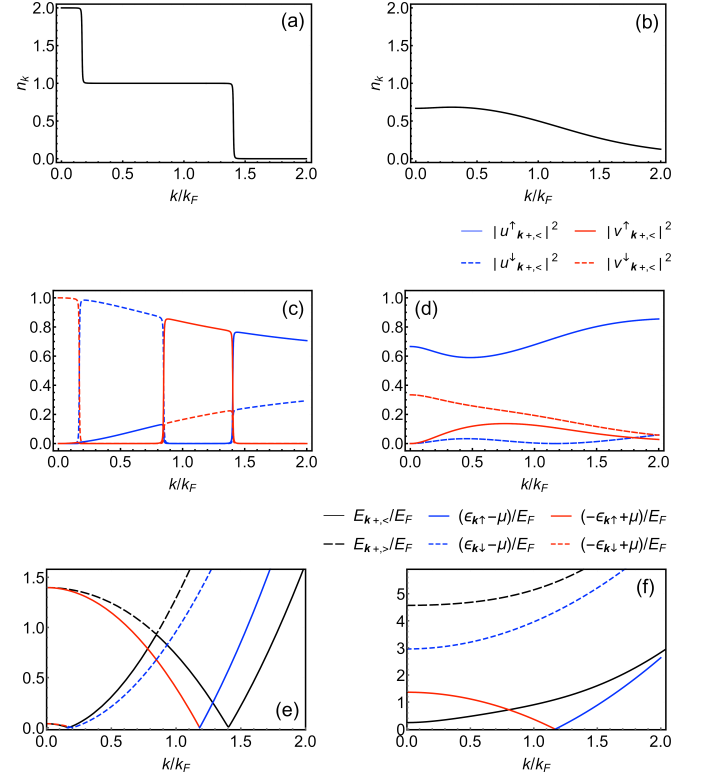


FIG. 9. Expected BCS and BEC characteristics are exhibited in the nontopological-superfluid (NSF) phase of a spin-orbit-coupled 2D Fermi gas. All results plotted here have been obtained for fixed $\lambda k_F/E_F = 0.75$, and $k \equiv |\mathbf{k}|$ is the magnitude of the 2D wave vector of Bogoliubov quasiparticles. Panels (a), (c) and (e) depict the BCS regime, showing results for $E_b/E_F = 0.010$ and $h = h_c - 0.04 E_F$. Juxtaposed are panels (b), (d) and (f) associated with the BEC regime, specifically for $E_b/E_F = 3.0$ and $h = h_<$ (corresponding to the filled circle with maximum h in Fig. 7). The presence [absence] of Fermi-surface features in the momentum-space density distribution n_k displayed in panel (a) [(b)] is typical for the BCS [BEC] regime of s -wave pairing. Also the k dependence of spin-resolved Bogoliubov amplitudes shown in panels (c) and (d) exhibits the familiar pattern, with the spin- \uparrow Nambu-particle component becoming dominant in the BEC regime. The quasiparticle dispersion $E_{k+,<}$ in the BCS regime [shown in panel (e)] has two minima corresponding to excitation gaps at finite k but, as expected, the excitation gap is at $k = 0$ in the BEC regime [see panel (f)]. Abrupt changes in the spin-resolved Bogoliubov amplitudes in the BCS regime [panel (c)] are the result of small-gap anticrossings between highly spin-polarized dispersion branches. We illustrate this by showing also the purely Zeeman-split dispersions $|\epsilon_{k\sigma} - \mu|$, which quite closely resemble the full dispersions $E_{k+,<}$ in the BCS regime [panel (e)]. In contrast, $E_{k+,<}$ is qualitatively different from $|\epsilon_{k\uparrow} - \mu|$ in the BEC regime [panel (f)].

shape [35–40]. This exact scenario is played out for our more complicated system of interest in the NSF phase. See Fig. 9 and the extensive discussion in its caption. In contrast, as illustrated by Fig. 10, all features associated with effective chiral p -wave pairing in the spin- \uparrow channel remain present throughout the BCS-to-BEC crossover in

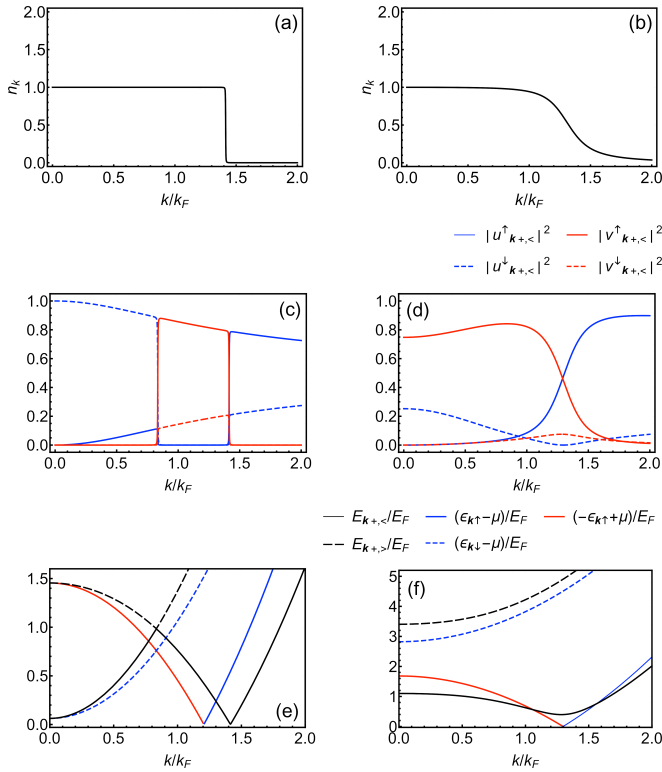


FIG. 10. Canonical features of chiral p -wave pairing persist in the topological-superfluid (TSF) phase of a spin-orbit-coupled 2D Fermi gas throughout the BCS-to-BEC crossover of the underlying s -wave pairing. Results plotted here have been obtained for fixed $\lambda k_F/E_F = 0.75$, and $k \equiv |\mathbf{k}|$ is the magnitude of the 2D wave vector of Bogoliubov quasiparticles. Panels (a), (c) and (e) depict the BCS regime ($E_b/E_F = 0.010$ and $h = h_c + 0.04 E_F$), whereas panels (b), (d) and (f) are associated with the BEC regime ($E_b/E_F = 3.0$ and $h = h_>$, corresponding to the filled square with minimum h in Fig. 7). The momentum-space density distribution n_k has the same distinctive Fermi-surface feature in both the BCS and BEC regimes of the TSF [see panels (a) and (b)]. Panel (c) [(d)] shows the spin-resolved particle and hole probability densities for the lowest positive-energy branch $E_{k+,<}$ of Bogoliubov-quasiparticle excitations whose energy dispersion is the black solid curve in panel (e) [(f)]. Unlike in the BEC regime for the NSF [refer to Fig. 9(d)], both spin- \uparrow -particle and spin- \uparrow -hole amplitudes dominate in the BEC regime of the TSF [depicted here in panel (d)]. The purity of this realization of chiral- p -wave pairing contrasts with the complicated pattern of the spin-resolved Bogoliubov amplitudes in the BCS regime [panel (c)], which is the result of small-gap anticrossings between several highly spin-polarized dispersion branches. For illustration, panels (e) and (f) also show the purely Zeeman-split dispersions $|\epsilon_{k\sigma} - \mu|$.

the TSF phase. In particular, the momentum-space density distribution shows a distinctive Fermi-surface edge feature even deep in the BEC regime for s -wave pairing, which is unexpected for situations where the chemical potential is negative [68]. That the effective p -wave pairing retains BCS-like behavior even as the underlying s -wave

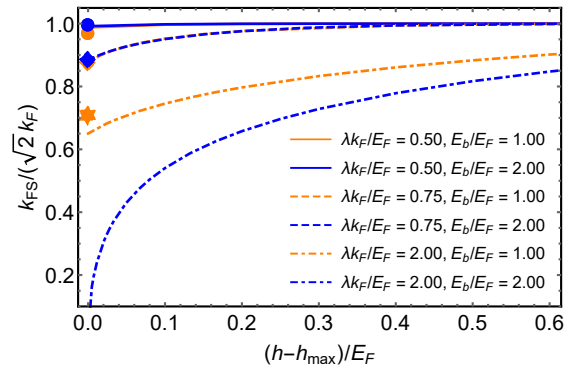


FIG. 11. Radius k_{FS} of the Fermi surface emerging in the topological-superfluid (TSF) phase of a spin-orbit-coupled 2D Fermi gas with density $n = mE_F/(\pi\hbar^2) \equiv k_F^2/(2\pi)$ subject to s -wave pairing in the BEC regime, defined formally via the condition (10). The parameter $\lambda k_F/E_F$ measures the spin-orbit-coupling strength, E_b is the s -wave two-particle bound-state energy, and h_{max} corresponds to the critical Zeeman energy above which the system's ground state is a uniform TSF. The two circles (diamonds) indicate values predicted for $k_{FS}(h_{max})$ by Eq. (3), which is expected to be valid for $\lambda k_F < h_{max}$, using $\lambda k_F/E_F = 0.50$ (0.75) and E_b/E_F associated with the correspondingly colored solid (dashed) line. The orange star indicates the value based on the estimate $k_{FS}(h_{max}) \approx \lambda k_F/(2E_F)$ that is expected to apply when $h_{max} < \lambda k_F$ concomitantly with $\lambda k_F/E_F \gtrsim 1$, which is the case for the parameters of the orange dot-dashed curve.

pairing is in the BEC regime is illustrated most strikingly by the close resemblance between the true Bogoliubov-quasiparticle energies and the dispersions associated with unpaired fermions [see Fig. 10(f)]. Although much larger generically than in the BCS regime, Δ_{pw} in the TSF phase for large E_b/E_F is still small enough because of its dependence on the inverse of the Zeeman energy [see Eq. (2)] that the resulting quasiparticle dispersions are not radically different from those obtained in the absence of pairing. This contrasts with the NSF phase occurring at lower h for the same large value of E_b/E_F where the unpaired-fermion dispersions are not at all representative of the lowest-energy branch of quasiparticle excitations [see Fig. 9(f)].

The stabilization of the Fermi surface in the TSF phase due to the larger Zeeman energy is demonstrated in Fig. 11. Here we plot the h dependence of the Fermi-surface radius k_{FS} , where the latter is defined as the location of the crossing point of the spin- \uparrow -particle and spin- \uparrow -hole Bogoliubov-spinor magnitudes for the lowest-energy quasiparticle dispersion,

$$|u_{\mathbf{k}+,<}^{\uparrow}|_{|\mathbf{k}|=k_{FS}}^2 = |v_{\mathbf{k}+,<}^{\uparrow}|_{|\mathbf{k}|=k_{FS}}^2 \quad (10)$$

The condition $|\mathbf{k}| = k_{FS}$ clearly defines a surface in wave-vector space that separates states having high and low occupation probabilities, which is the defining property of a Fermi surface [35]. We find that a crossing point yielding a definite value of k_{FS} always exists at $h \geq h_{max}$

for any values of E_b/E_F and $\lambda k_F/E_F$. For $\lambda k_F/E_F < 1$, the minimum in the dispersion curve $E_{\mathbf{k}_{+,<}}$ also occurs at $|\mathbf{k}| = k_{\text{FS}}$, and the latter's value turns out to be well-approximated by Eq. (3) for $\lambda k_F < h_{\text{max}}$. In situations with very large spin-orbit coupling $\lambda k_F/E_F \gtrsim 1$, the dispersion minimum is observed to sometimes be absent or appear at $|\mathbf{k}| \neq k_{\text{FS}}$ right after the transition to the TSF phase. Nevertheless, the coincidence of the quasiparticle-dispersion minimum and k_{FS} is established for $h \gtrsim h_{\text{max}}$ even in such cases. Application of the approximate two-band-model results from Ref. 13 to the case $\lambda k_F > h_{\text{max}}$ yields a conservative estimate for the Fermi-surface radius in this regime, which is given by

$$\frac{k_{\text{FS}}}{k_F} = \frac{\lambda k_F}{2E_F} + \sqrt{\frac{\mu}{E_F} + \frac{\lambda^2 k_F^2}{4E_F^2} + \frac{|\Delta|^2}{E_F^2} \left(\frac{E_F}{\sqrt{2}\lambda k_F} - \frac{E_F}{h} \right)} \quad (11)$$

and only holds when the expression under the square-root is positive. According to results presented in Fig. 11, k_{FS} increases monotonically as a function of $h - h_{\text{max}}$ until reaching its asymptotic value $\sqrt{2} k_F$, which corresponds to the Fermi-surface radius of a spin-polarized 2D Fermi gas with density $n \equiv k_F^2/(2\pi)$.

As can be seen in Fig. 10, the most visible attributes that distinguish the TSF in the BEC regime from that arising in the BCS regime are the increased magnitude of the low-energy excitation gap Δ_{pw} and the strong suppression of the minority-spin degrees of freedom. The clear dominance of the spin- \uparrow Bogoliubov amplitudes representing chiral p -wave pairing is one of the favorable qualities exhibited by the TSF realized in the BEC regime. In addition, a larger magnitude of Δ_{pw} should help to reduce the influence of many experimental nonidealities, including thermal fluctuations, as long as E_b/E_F is not too large so that beyond-mean-field fluctuations have not yet significantly suppressed the value of the pairing gap. Thus, the TSF realized in the onset of the BEC regime of the underlying s -wave pairing constitutes both a purer and more-robust version of the highly sought-after chiral p -wave order.

The results obtained and conclusions drawn in our work are based on the application of mean-field theory. It is well-known that this method can only provide limited insight into the strongly interacting (i.e., the BEC) regime of 2D systems [39, 40, 46–50]. Here we employed the mean-field approach to determine (i) the phase diagram, (ii) the magnitude of the pairing gap, and (iii) momentum-space density distributions. Before concluding, we discuss the reliability of our predictions for these three purposes. (i) *Phase diagrams*: It is generally accepted that zero-temperature phase diagrams obtained within mean-field theory are qualitatively correct, even in the BEC regime [9, 30, 43–45]. We therefore expect the features presented in our work to be similarly accurate. (ii) *Pairing-gap magnitude*: Suppression of the pairing gap by beyond-mean-field fluctuations becomes increasingly important for larger E_b [49, 51]. Therefore, results for gap magnitudes presented, e.g., in Fig. 2 are

only reliable for $E_b/E_F \lesssim 1$. Nevertheless, the conclusion that $E_b/E_F \sim 1$ is optimal for realizing a robust TSF continues to hold. (iii) *Momentum-space density distributions*: Recent numerical results obtained for our system of interest in the $h = 0$ limit (see Supplemental Material for Ref. [40]) indicate that momentum-space density distributions obtained within mean-field theory are accurate to within $\lesssim 10\%$. Thus our general conclusions about the re-emergence of a Fermi surface and the robustness of chiral p -wave superfluidity in the BEC regime of s -wave pairing are expected to be valid.

IV. CONCLUSIONS AND OUTLOOK

We have investigated the strongly interacting regime of the 2D Fermi gas with s -wave pairing, with fixed particle density and subject to both spin-orbit coupling and Zeeman spin splitting. Characteristic features of the phase diagram as a function of two-particle binding energy E_b and Zeeman energy h are elucidated and the properties of the homogeneous superfluid phases studied in greater detail. In particular, we tracked the boundaries of the homogeneous nontopological and topological superfluids. The second-order topological-transition line $h_c(E_b)$, with h_c defined via Eq. (1), is truncated by a phase-separation region that emerges for E_b larger than a critical value $E_b^{(c)}$ that depends on the spin-orbit-coupling strength (see Figs. 1 and 8). As a result, the topological transition is of first order in the limit of large E_b/E_F .

The homogeneous nontopological phase exhibits all of the expected features commonly associated with the BCS-to-BEC crossover for s -wave pairing, especially the shrinking, and eventual disappearance, of an underlying Fermi surface as the Cooper-pair binding energy is increased. See Fig. 9(a,b). In contrast, as illustrated in Fig. 10, the topological superfluid phase always retains the basic properties of the BCS regime, including the Fermi-surface characteristics, even for large E_b/E_F . This effect demonstrates the continuity of topological protection through the BCS-to-BEC crossover. The larger the value of $\lambda k_F/E_F$, the smaller is the Fermi-surface radius k_{FS} at the transition point $h = h_{\text{max}}$ into the uniform topological phase. With increasing $h > h_{\text{max}}$, the Fermi surface is enlarged until its radius reaches the asymptotic value $\sqrt{2} k_F$ expected for a spin-polarized 2D Fermi sea with density $n \equiv k_F^2/(2\pi)$. See Fig. 11 for an illustration.

Promising first steps have recently been made towards physical realization of our system of interest by demonstrating essential ingredients, e.g., in ultra-cold-atom gases [69] and solid-state heterostructures [70, 71]. State-of-the-art experimental techniques [72] could be utilized, or related theoretical proposals [73] may be pursued, to confirm the re-appearance of a Fermi surface as the Zeeman energy is tuned across the topological transition when the system is in the BEC regime of the underlying s -wave pairing. Compared to the BCS regime, chiral p -wave superfluidity realized in the BEC

regime has a larger excitation gap and is less obscured by minority-spin degrees of freedom, making it the ideal platform for exploring exotic Majorana excitations in vortices [18–20] and their potential use for topological quantum-information-processing paradigms [22]. Future work could focus on elucidating also the evolution and properties of topological superfluids within the phase-separation region.

ACKNOWLEDGMENTS

U.Z. thanks W. Belzig, C. Bruder, M. M. Parish, D. M. Stamper-Kurn, and O. P. Sushkov for useful discussions. This work was supported by the Marsden Fund Council (contract no. MAU1604), from NZ government funding managed by the Royal Society Te Apārangi.

-
- [1] M. Sato and Y. Ando, “Topological superconductors: a review,” *Rep. Prog. Phys.* **80**, 076501 (2017).
- [2] L. Fu and C. L. Kane, “Superconducting proximity effect and Majorana fermions at the surface of a topological insulator,” *Phys. Rev. Lett.* **100**, 096407 (2008).
- [3] C. Zhang, S. Tewari, R. M. Lutchyn, and S. Das Sarma, “ $p_x + ip_y$ superfluid from s-wave interactions of fermionic cold atoms,” *Phys. Rev. Lett.* **101**, 160401 (2008).
- [4] J. D. Sau, R. M. Lutchyn, S. Tewari, and S. Das Sarma, “Generic new platform for topological quantum computation using semiconductor heterostructures,” *Phys. Rev. Lett.* **104**, 040502 (2010).
- [5] J. Alicea, “Majorana fermions in a tunable semiconductor device,” *Phys. Rev. B* **81**, 125318 (2010).
- [6] M. Sato, Y. Takahashi, and S. Fujimoto, “Non-Abelian topological orders and Majorana fermions in spin-singlet superconductors,” *Phys. Rev. B* **82**, 134521 (2010).
- [7] B. S. Chandrasekhar, “A note on the maximum critical field of high-field superconductors,” *Appl. Phys. Lett.* **1**, 7 (1962).
- [8] A. M. Clogston, “Upper limit for the critical field in hard superconductors,” *Phys. Rev. Lett.* **9**, 266 (1962).
- [9] L. He and P. Zhuang, “Phase diagram of a cold polarized Fermi gas in two dimensions,” *Phys. Rev. A* **78**, 033613 (2008).
- [10] Yu. A. Bychkov and E. I. Rashba, “Properties of a 2D electron gas with lifted spectral degeneracy,” *Pis'ma Zh. Eksp. Teor. Fiz.* **39**, 66 (1984), [*JETP Lett.* **39**, 78 (1984)].
- [11] R. Winkler, *Spin-Orbit Coupling Effects in Two-Dimensional Electron and Hole Systems* (Springer, Berlin, 2003).
- [12] V. Galitski and I. B. Spielman, “Spin-orbit coupling in quantum gases,” *Nature (London)* **494**, 49 (2013).
- [13] J. Brand, L. A. Toikka, and U. Zülicke, “Accurate projective two-band description of topological superfluidity in spin-orbit-coupled Fermi gases,” *SciPost Phys.* **5**, 16 (2018).
- [14] C. Kallin and J. Berlinsky, “Chiral superconductors,” *Rep. Prog. Phys.* **79**, 054502 (2016).
- [15] R. Jackiw and C. Rebbi, “Solitons with fermion number $\frac{1}{2}$,” *Phys. Rev. D* **13**, 3398–3409 (1976).
- [16] N. B. Kopnin and M. M. Salomaa, “Mutual friction in superfluid ^3He : Effects of bound states in the vortex core,” *Phys. Rev. B* **44**, 9667–9677 (1991).
- [17] G. E. Volovik, “Fermion zero modes on vortices in chiral superconductors,” *JETP Lett.* **70**, 609–614 (1999).
- [18] N. Read and D. Green, “Paired states of fermions in two dimensions with breaking of parity and time-reversal symmetries and the fractional quantum Hall effect,” *Phys. Rev. B* **61**, 10267–10297 (2000).
- [19] D. A. Ivanov, “Non-Abelian statistics of half-quantum vortices in p -wave superconductors,” *Phys. Rev. Lett.* **86**, 268–271 (2001).
- [20] V. Gurarie and L. Radzihovsky, “Zero modes of two-dimensional chiral p -wave superconductors,” *Phys. Rev. B* **75**, 212509 (2007).
- [21] S. Tewari, S. Das Sarma, and D.-H. Lee, “Index theorem for the zero modes of Majorana fermion vortices in chiral p -wave superconductors,” *Phys. Rev. Lett.* **99**, 037001 (2007).
- [22] S. Das Sarma, M. Freedman, and C. Nayak, “Majorana zero modes and topological quantum computation,” *npj Quant. Inf.* **1**, 15001 (2015).
- [23] F. Loder, A. P. Kampf, and T. Kopp, “Route to topological superconductivity via magnetic field rotation,” *Sci. Rep.* **5**, 15302 (2015).
- [24] H. Zhai, “Degenerate quantum gases with spin-orbit coupling: a review,” *Rep. Prog. Phys.* **78**, 026001 (2015).
- [25] W. Zhang, W. Yi, and C. A. R. Sá de Melo, eds., *Synthetic Spin-Orbit Coupling in Cold Atoms* (World Scientific, Singapore, 2018).
- [26] A. J. Leggett, “Diatomic molecules and Cooper pairs,” in *Modern Trends in the Theory of Condensed Matter*, edited by A. Pękalski and J. A. Przystawa (Springer, Berlin, 1980) pp. 13–27.
- [27] A. J. Leggett, “Cooper pairing in spin-polarized Fermi systems,” *J. Phys. Colloques* **41**(C7), 19–26 (1980).
- [28] M. Randeria, J.-M. Duan, and L.-Y. Shieh, “Superconductivity in a two-dimensional Fermi gas: Evolution from Cooper pairing to Bose condensation,” *Phys. Rev. B* **41**, 327–343 (1990).
- [29] M. M. Parish, “The BCS–BEC crossover,” in *Quantum Gas Experiments*, edited by P. Törmä and K. Sengstock (Imperial College Press, London, 2015) pp. 179–197.
- [30] G. C. Strinati, P. Pieri, G. Röpke, P. Schuck, and M. Urban, “The BCS–BEC crossover: From ultra-cold Fermi gases to nuclear systems,” *Phys. Repts.* **738**, 1–76 (2018).
- [31] The energy E_b measures the strength of particle-particle interactions and corresponds to the dimer binding energy in the absence of spin-orbit coupling [24]. For zero-range interactions, it is related to the 2D s -wave scattering length a_{2D} by $E_b = \hbar^2/(m a_{2D})$ [74, 75], although different conventions for defining the scattering length have been adopted in the literature [76].
- [32] W. Yi and G.-C. Guo, “Phase separation in a polarized Fermi gas with spin-orbit coupling,” *Phys. Rev. A* **84**, 031608 (2011).
- [33] X. Yang and S. Wan, “Phase diagram of a uniform two-dimensional Fermi gas with spin-orbit coupling,” *Phys. Rev. A* **85**, 023633 (2012).
- [34] See, e.g., Fig. 2(a) in Ref. [9].

- [35] R. Sensarma, M. Randeria, and N. Trivedi, “Can one determine the underlying Fermi surface in the superconducting state of strongly correlated systems?” *Phys. Rev. Lett.* **98**, 027004 (2007).
- [36] P. Nozières and S. Schmitt-Rink, “Bose condensation in an attractive fermion gas: From weak to strong coupling superconductivity,” *J. Low Temp. Phys.* **59**, 195–211 (1985).
- [37] Q. Chen, J. Stajic, S. Tan, and K. Levin, “BCS–BEC crossover: From high temperature superconductors to ultracold superfluids,” *Phys. Rep.* **412**, 1–88 (2005).
- [38] G. E. Astrakharchik, J. Boronat, J. Casulleras, and S. Giorgini, “Momentum distribution and condensate fraction of a fermion gas in the BCS-BEC crossover,” *Phys. Rev. Lett.* **95**, 230405 (2005).
- [39] H. Shi, S. Chiesa, and S. Zhang, “Ground-state properties of strongly interacting Fermi gases in two dimensions,” *Phys. Rev. A* **92**, 033603 (2015).
- [40] H. Shi, P. Rosenberg, S. Chiesa, and S. Zhang, “Rashba spin-orbit coupling, strong interactions, and the BCS-BEC crossover in the ground state of the two-dimensional Fermi gas,” *Phys. Rev. Lett.* **117**, 040401 (2016).
- [41] K. Seo, L. Han, and C. A. R. Sá de Melo, “Topological phase transitions in ultracold Fermi superfluids: The evolution from Bardeen-Cooper-Schrieffer to Bose-Einstein-condensate superfluids under artificial spin-orbit fields,” *Phys. Rev. A* **85**, 033601 (2012).
- [42] L. He and X.-G. Huang, “Superfluidity and collective modes in Rashba spin-orbit coupled Fermi gases,” *Ann. Phys. (Leipzig)* **337**, 163–207 (2013).
- [43] W. Yi and L.-M. Duan, “Phase diagram of a polarized Fermi gas across a Feshbach resonance in a potential trap,” *Phys. Rev. A* **74**, 013610 (2006).
- [44] M. M. Parish, F. M. Marchetti, A. Lamacraft, and B. D. Simons, “Finite-temperature phase diagram of a polarized Fermi condensate,” *Nat. Phys.* **3**, 124–128 (2007).
- [45] A. M. Fischer and M. M. Parish, “BCS-BEC crossover in a quasi-two-dimensional Fermi gas,” *Phys. Rev. A* **88**, 023612 (2013).
- [46] M. Yu. Kuchiev and O. P. Sushkov, “Many-body correlation corrections to superconducting pairing in two dimensions,” *Phys. Rev. B* **53**, 443–448 (1996).
- [47] G. Bertaina and S. Giorgini, “BCS-BEC crossover in a two-dimensional Fermi gas,” *Phys. Rev. Lett.* **106**, 110403 (2011).
- [48] L. Salasnich and F. Toigo, “Composite bosons in the two-dimensional BCS-BEC crossover from Gaussian fluctuations,” *Phys. Rev. A* **91**, 011604 (2015).
- [49] L. He, H. Lü, G. Cao, H. Hu, and X.-J. Liu, “Quantum fluctuations in the BCS-BEC crossover of two-dimensional Fermi gases,” *Phys. Rev. A* **92**, 023620 (2015).
- [50] A. V. Turlapov and M. Yu. Kagan, “Fermi-to-Bose crossover in a trapped quasi-2D gas of fermionic atoms,” *J. Phys.: Condens. Matter* **29**, 383004 (2017).
- [51] H. Hu, B. C. Mulkerin, L. He, J. Wang, and X.-J. Liu, “Quantum fluctuations of a resonantly interacting p -wave Fermi superfluid in two dimensions,” *Phys. Rev. A* **98**, 063605 (2018).
- [52] P. G. de Gennes, *Superconductivity of Metals and Alloys* (Addison-Wesley, Reading, MA, 1989).
- [53] Our notation adheres to that used in Ref. [13].
- [54] While we adopt the 2D-Rashba form [10] for $\lambda_{\mathbf{k}}$, our results apply also to other types of spin-orbit coupling that depend linearly on the components of \mathbf{k} , such as the 2D-Dirac and 2D-Dresselhaus functional forms [11, 12] corresponding to $\lambda_{\mathbf{k}} = \lambda(k_x - ik_y)$ and $\lambda(k_x + ik_y)$, respectively.
- [55] J. Zhou, W. Zhang, and W. Yi, “Topological superfluid in a trapped two-dimensional polarized Fermi gas with spin-orbit coupling,” *Phys. Rev. A* **84**, 063603 (2011).
- [56] L. Radzihovsky and D. E. Sheehy, “Imbalanced Feshbach-resonant Fermi gases,” *Rep. Prog. Phys.* **73**, 076501 (2010).
- [57] D. E. Sheehy and L. Radzihovsky, “BEC–BCS crossover, phase transitions and phase separation in polarized resonantly-paired superfluids,” *Ann. Phys. (NY)* **322**, 1790–1924 (2007).
- [58] D. E. Sheehy and L. Radzihovsky, “Comment on “Superfluid stability in the BEC-BCS crossover”,” *Phys. Rev. B* **75**, 136501 (2007).
- [59] G. Sarma, “On the influence of a uniform exchange field acting on the spins of the conduction electrons in a superconductor,” *J. Phys. Chem. Solids* **24**, 1029–1032 (1963).
- [60] A. Lamacraft and F. M. Marchetti, “Spinodal decomposition in polarized Fermi superfluids,” *Phys. Rev. B* **77**, 014511 (2008).
- [61] L. He and P. Zhuang, “Stable Sarma state in two-band Fermi systems,” *Phys. Rev. B* **79**, 024511 (2009).
- [62] P. F. Bedaque, H. Caldas, and G. Rupak, “Phase separation in asymmetrical fermion superfluids,” *Phys. Rev. Lett.* **91**, 247002 (2003).
- [63] J. Carlson and S. Reddy, “Asymmetric two-component fermion systems in strong coupling,” *Phys. Rev. Lett.* **95**, 060401 (2005).
- [64] D. E. Sheehy and L. Radzihovsky, “BEC-BCS crossover in “magnetized” Feshbach-resonantly paired superfluids,” *Phys. Rev. Lett.* **96**, 060401 (2006).
- [65] D. T. Son and M. A. Stephanov, “Phase diagram of a cold polarized Fermi gas,” *Phys. Rev. A* **74**, 013614 (2006).
- [66] J.-J. Du, C. Chen, and J.-J. Liang, “Asymmetric two-component Fermi gas in two dimensions,” *Phys. Rev. A* **80**, 023601 (2009).
- [67] This task becomes particularly challenging for the part of the phase diagram where multiple selfconsistent solutions of the gap equation exist at fixed h . Generally, two of these correspond to minima of the ground-state energy taken at fixed μ , and their combined evolution between global- or local-minimum status needs to be tracked.
- [68] See, e.g., Ref. [37]. Similar behavior to the one found by us here for the 2D TSF seems to also be implicit in results that were presented for the 3D spin-orbit-coupled Fermi superfluid (see, e.g., Fig. 6 in Ref. [41]) but whose physical significance was not discussed.
- [69] Z. Meng, L. Huang, P. Peng, D. Li, L. Chen, Y. Xu, C. Zhang, P. Wang, and J. Zhang, “Experimental observation of a topological band gap opening in ultracold Fermi gases with two-dimensional spin-orbit coupling,” *Phys. Rev. Lett.* **117**, 235304 (2016).
- [70] M. Ben Shalom, M. Sachs, D. Rakhmilevitch, A. Palevski, and Y. Dagan, “Tuning spin-orbit coupling and superconductivity at the SrTiO₃/LaAlO₃ interface: A magnetotransport study,” *Phys. Rev. Lett.* **104**, 126802 (2010).
- [71] J. Shabani, M. Kjaergaard, H. J. Suominen, Y. Kim, F. Nichele, K. Pakrouski, T. Stankevic, R. M. Lutchyn, P. Krogstrup, R. Feidenhans’l, S. Kraemer, C. Nayak, M. Troyer, C. M. Marcus, and C. J.

- Palmstrøm, “Two-dimensional epitaxial superconductor-semiconductor heterostructures: A platform for topological superconducting networks,” *Phys. Rev. B* **93**, 155402 (2016).
- [72] C. A. Regal, M. Greiner, S. Giorgini, M. Holland, and D. S. Jin, “Momentum distribution of a Fermi gas of atoms in the BCS-BEC crossover,” *Phys. Rev. Lett.* **95**, 250404 (2005).
- [73] W. Yi and L.-M. Duan, “Detecting the breached-pair phase in a polarized ultracold Fermi gas,” *Phys. Rev. Lett.* **97**, 120401 (2006).
- [74] I. Bloch, J. Dalibard, and W. Zwerger, “Many-body physics with ultracold gases,” *Rev. Mod. Phys.* **80**, 885 (2008).
- [75] J. Levinsen and M. M. Parish, “Strongly interacting two-dimensional Fermi gases,” in *Annual Review of Cold Atoms and Molecules*, Vol. 3, edited by K. W. Madison, K. Bongs, L. D. Carr, A. M. Rey, and H. Zhai (World Scientific, Singapore, 2015) Chap. 1, pp. 1–75.
- [76] P. Jeszenszki, A. Yu. Cherny, and J. Brand, “s-wave scattering length of a Gaussian potential,” *Phys. Rev. A* **97**, 042708 (2018).